Applied Physics Letters

Three-dimensional Fermi surface and small effective masses in Mo_8Ga_{41}

Cite as: Appl. Phys. Lett. **116**, 202601 (2020); https://doi.org/10.1063/5.0005177
Submitted: 26 February 2020 . Accepted: 06 May 2020 . Published Online: 20 May 2020

Zhixiang Hu, D. Graf, Yu Liu, and C. Petrovic

Applied Physics Letters ARTICLE scitation.org/journal/apl

Three-dimensional Fermi surface and small effective masses in Mo_8Ga_{41}

Cite as: Appl. Phys. Lett. **116**, 202601 (2020); doi: 10.1063/5.0005177
Submitted: 26 February 2020 · Accepted: 6 May 2020 ·
Published Online: 20 May 2020

View Online Export Citation CrossMark

Zhixiang Hu,[1,2,a)] D. Graf,[3] Yu Liu,[1] and C. Petrovic[1,2,a)]

AFFILIATIONS

[1]Condensed Matter Physics and Materials Science Department, Brookhaven National Laboratory, Upton, New York 11973, USA
[2]Department of Physics and Astronomy, Stony Brook University, Stony Brook, New York 11794-3800, USA
[3]National High Magnetic Field Laboratory, Florida State University, Tallahassee, Florida 32306-4005, USA

[a)]Authors to whom correspondence should be addressed: zhixiang@bnl.gov and petrovic@bnl.gov

ABSTRACT

We report Fermi surface characteristics of Mo_8Ga_{41}, a two-gap superconductor with a critical temperature of $T_c \sim 10$ K, obtained from quantum oscillation measurements. Four major frequencies have been observed with relatively small quasiparticle masses. The angular dependence of major frequencies indicates three-dimensional Fermi surface sheets. This argues for a relatively isotropic superconducting state and, given its relatively high T_c, shows that a search for materials in this class could be of interest for superconducting wire applications.

Magnesium diboride with its superconducting critical temperature T_c similar to doped La_2CuO_4, rather simple crystallography and phonon-mediated superconductivity, stimulated considerable interest.[1,2] Indeed, recent years have reaffirmed that room-temperature superconductors should be sought among non-magnetic materials with high phonon frequencies[3–5] rather than in magnetic copper oxide ceramics and spin-fluctuation pairing mechanisms.[6]

Similar to MgB_2, Mo_8Ga_{41} is a binary intermetallic superconductor. Its superconducting $T_c = 9.7$ K, and upper critical field $\mu_0 H_{c2} = 8.36$ T.[7] It has been pointed out that, like MgB_2, Mo_8Ga_{41} is also on the verge of a structural instability[8,9] and exhibits strong-coupling two-gap BCS superconductivity and good flux pinning potential.[10–15] In light of the relatively high critical temperature and upper critical field, further studies of this material are highly desirable.

Fermi surface characteristics give insight into conducting states that are subject to Cooper pairing and are rather important for predictive materials design.[16–19] In this work, we have performed a comprehensive quantum oscillation study of Mo_8Ga_{41}. Multiple Fermi surface sheets with three-dimensional characteristics have been found with rather small quasiparticle masses. Three-dimensional Fermi surfaces and two-band superconductivity argue in favor of further search for materials in this class for superconducting wire applications.[20,21]

Single crystals of Mo_8Ga_{41} were grown by the high temperature self-flux method.[22] Mo and Ga were mixed in a ratio of 8:500 in an alumina crucible and sealed in evacuated quartz tube. The ampoule was heated up to 850° in two hours, held at 850 °C for 10 h, and then slowly cooled to 170 °C for 55 h, where crystals were decanted. Residual gallium was removed by crystal etching in diluted hydrochloric acid. X-ray diffraction (XRD) was performed on crushed crystals at room temperature by using Cu–K_α ($\lambda = 0.15418$ nm) radiation in a Rigaku Miniflex powder diffractometer. The chemical composition was verified by energy-dispersive x-ray spectroscopy (EDX) in a JEOL LSM-6500 scanning electron microscope. Magnetic susceptibility was measured in the zero-field cooling mode using a Quantum Design MPMS-5XL. The de Haas van Alphen (dHvA) oscillation experiments were performed at NHMFL Tallahassee. The crystals were mounted onto miniature Seiko piezoresistive cantilevers that were installed on a rotating platform. The field direction can be changed continuously between parallel ($\theta = 0°$) and perpendicular ($\theta = 90°$) to the *ab*-plane of the crystal. The average inverse magnetic field was determined from $(H_{max}^{-1} + H_{min}^{-1})/2$.

The powder x-ray diffraction (XRD) pattern [Fig. 1(a)] confirms that single crystals crystallize in a *R* -3*h* space group. The refined lattice parameters are $a = b = 1.4031(2)$ nm and $c = 1.5042(2)$ nm in agreement with the reported values.[23] Figure 1(b) shows the typical crystal size, about two times larger than that previously reported.[10] EDX shows a stoichiometric ratio of 0.167:0.833, which is close to the Mo:Ga ratio of 8:41. The crystal structure of Mo_8Ga_{41} consists of stacked $MoGa_{10}$ Mo–Ga polyhedral cages with Mo atoms at the center, with two different atomic positions for Mo and nine for Ga

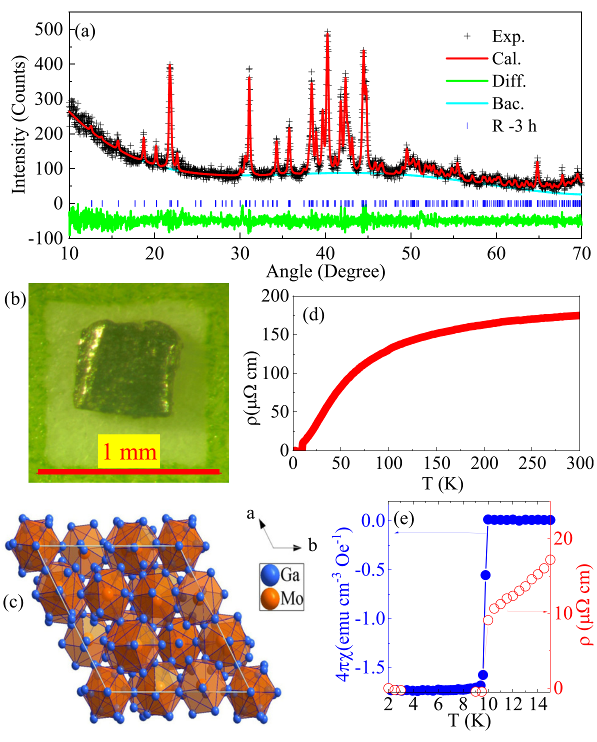

FIG. 1. (a) Powder XRD pattern and refinement results. The data are shown by (+); fitting, difference, and background curves are given by the red, green, and blue solid lines, respectively. Single crystals (b) and crystal structure (c) of Mo_8Ga_{41}. (d) Temperature dependence of the in-plane resistivity. (e) Superconducting T_c measured by in-plane magnetic susceptibility in a magnetic field of 10 Oe and zero-field resistivity, indicating $T_c = 9.8(1)$ K.

[Fig. 1(c)].[10,23] Resistivity shows the absence of phase transition above superconducting T_c, residual resistivity ratio of $\mathrm{RRR} = \rho(300\,\mathrm{K})/\rho(10\,\mathrm{K}) = 17$, and $\rho(10\,\mathrm{K}) = 10\ \mu\Omega$ cm [Fig. 1(d)]. Superconducting T_c inferred from the diamagnetic signal of our crystals [Fig. 1(e)] is consistent with that of polycrystalline Mo_8Ga_{41}.[7]

The field-dependent cantilever signal [Fig. 2(a)] in the magnetic field applied perpendicular to the *c*-axis shows clear dHvA oscillations above 10 T. The cantilever signal and dHvA amplitude increase in the magnetic field at all temperatures. Oscillating part of the signal and its Fast Fourier Transform (FFT) [Figs. 2(b) and 2(c)] show sharp peaks. The peaks correspond to the orthogonal cross-sectional area of the Fermi surface (FS) A_F, as described by the Onsager relation $F = (\Phi_0/2\pi^2)A_F$, where Φ_0 is the flux quantum. Therefore, we estimate $A_{F\alpha} = 7.88(1)\,\mathrm{nm}^{-2}$, $A_{F\beta} = 4.85(1)\,\mathrm{nm}^{-2}$, $A_{F\gamma} = 1.18(1)\,\mathrm{nm}^{-2}$, and $A_{F\delta} = 1.98(1)\,\mathrm{nm}^{-2}$ for background subtraction-independent frequencies $F_\alpha = 826.9$ T, $F_\beta = 508.3$ T, $F_\gamma = 124.4$ T, and $F_\delta = 204.7$ T, respectively. The effective cyclotron mass of carriers at observed Fermi surface sheets is obtained from the temperature dependence of FFT amplitude from the Lifshitz–Kosevich (LK) formula,[24,25]

$$FFT\ amp. \propto \frac{\alpha m^* T/H}{\sinh(\alpha m^* T/H)},$$

where $\alpha = 2\pi^2 K_B/e\hbar \approx 14.69$ T/K and $m^* = m/m_e$ is the effective cyclotron mass. The effective masses are estimated [Fig. 2(d)] to be

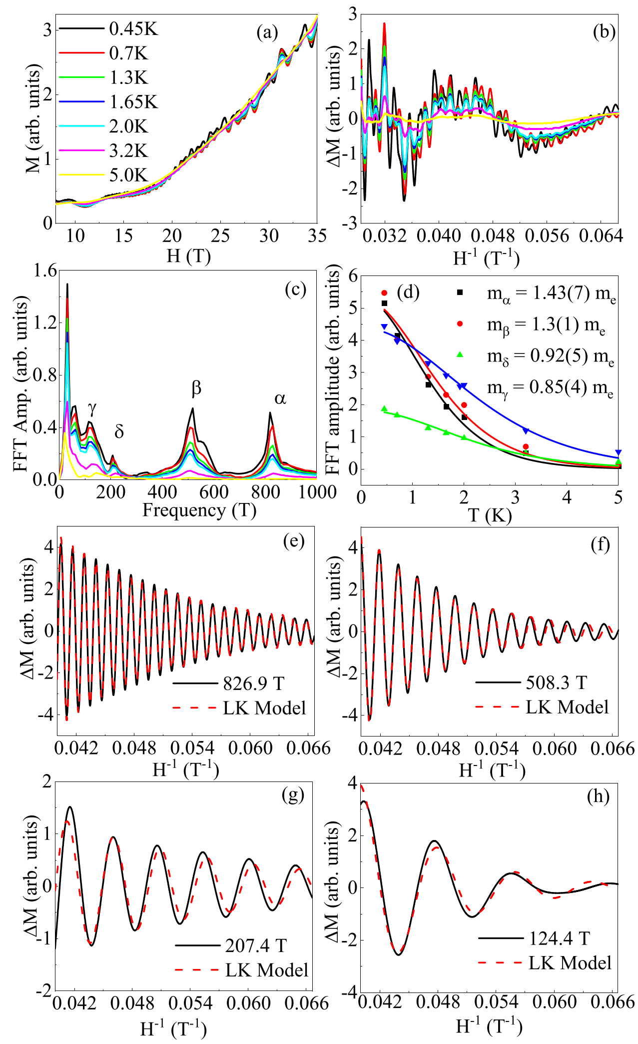

FIG. 2. (a) Temperature-dependent cantilever response of Mo_8Ga_{41} vs magnetic field, with the field applied perpendicular to the *c* axis. (b) Oscillatory component obtained by smooth background subtraction. (c) FFT spectrum of oscillations vs frequency with observed frequencies α, β, γ, and δ at different temperatures. Their effective masses are evaluated by using the Lifshitz–Kosevich (LK) formula (d). (e)–(h) Magnetic field-dependent amplitudes of characteristic frequencies.

$1.43(7)m_e$, $1.3(1)m_e$, $0.85(4)m_e$, and $0.92(5)m_e$ for Fermi surface parts that correspond to F_α, F_β, F_γ, and F_δ, respectively.

We obtain Dingle temperature by using the Lifshitz–Kosevich formula to fit the field-dependent amplitudes at 0.45 K for oscillation frequencies.[25–27] This gives Figs. 1(e)–1(h). $T_{D\alpha} = 3.00(1)$ K, $T_{D\beta} = 5.02(3)$ K, $T_{D\gamma} = 8.38(8)$ K, and $T_{D\delta} = 3.2(1)$ K.

Dingle temperature T_D is associated with the mean free path and the scattering rate τ via $T_D = \frac{\hbar}{2\pi k_B \tau_Q}$ that describes scattering of carriers due to particle interactions and defects inside the material. Differences in T_D among characteristic frequencies imply different quasiparticle lifetimes of Fermi surface sheets: $\tau_\alpha = 4.0(1) \times 10^{-13}$ s, $\tau_\beta = 2.4(1) \times 10^{-13}$ s, $\tau_\gamma = 1.4(1) \times 10^{-13}$ s, and $\tau_\delta = 3.8(1) \times 10^{-13}$ s. We can also approximate Fermi wave vector

$k_{F,\alpha} = 0.158(1)$ Å^{-1}, $k_{F,\beta} = 0.124(1)$ Å^{-1}, $k_{F,\gamma} = 0.061(1)$ Å^{-1}, and $k_{F,\delta} = 0.079(1)$ Å^{-1} assuming circular cross section $A_F = \pi k_F^2$. Mobility estimate using $\mu = e\tau/m_c$ gives 498.0 cm^2 V^{-1} s^{-1}, 327 cm^2 V^{-1} s^{-1}, 300.0 cm^2 V^{-1} s^{-1}, and 726.0 cm^2 V^{-1} s^{-1} for F_α, F_β, F_γ, and F_δ, respectively.

Angular-dependent dHvA oscillations were also measured. The crystal was rotated from −9°. The dHvA oscillations appear [Fig. 3(a)] at all angles above 10 T. Figure 3(b) shows FFT of the dHvA response. Traces of two frequencies, α and β, are clearly resolved and are plotted in Fig. 3(c). Frequency α shows oscillatory behavior with maxima at 45° and 110°. Frequency β increases through small angles (<30°), reaches the maximum also around 45°, and then decreases. The angular dependence of F_β can be described by the ellipsoidal fit[28] $F(\theta) = F_0[\cos^2(\theta) + (k_F^a/k_F^c)^2 \sin^2(\theta)]^{-1/2}$ [Fig. 3(c)]. The ratio of $(k_F^a/k_F^c) = 0.42(3)$ describes the eccentricity of the Fermi surface sheet associated with F_β.

The three-dimensional (3D) crystal structure of Mo_8Ga_{41} should result in rather dispersive bands in momentum space. Interestingly, the band structure of Mo_8Ga_{41} features narrow band dispersion, whereas the density of states at the Fermi level is dominated by Mo 4*d* and Ga4*p* orbital hybridization.[12] The 3D character of dHvA oscillations is consistent with first principles calculations[13] where four different bands cross the Fermi level. Based on the effective masses obtained in our experiment, it is reasonable for α and β frequencies with the electron pocket near the Brillouin zone corner and large anisotropic part of the Fermi surface, respectively, whereas other frequencies probably arise due to the band associated with two hole pockets near the Γ point, which exhibit weak coupling with phonons and where the superconducting gap is smaller.[13] Therefore, bands corresponding to α and β Fermi surface sheets that exhibit a larger superconducting gap feature three-dimensional characteristics.

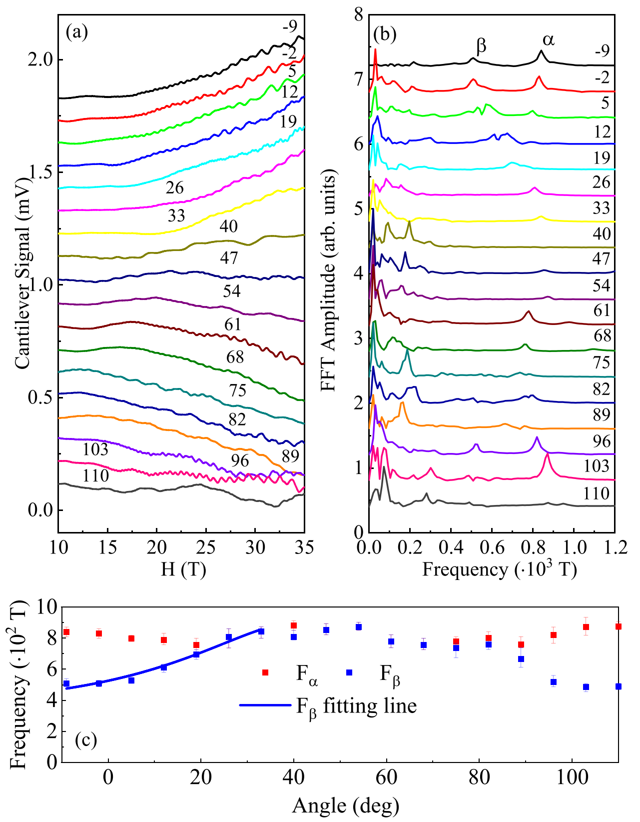

FIG. 3. (a) Angle-dependent dHvA oscillations vs magnetic field with offset for clarity. The field was applied along the *c* axis, and the sample was rotated from −9° to 110°; (b) FFT of response $\Delta V = V - \langle V \rangle$ vs frequency at different angles; (c) traces of frequencies α and β with the angle fitted with the ellipsoid model.

In conclusion, we present the experimental study of the Fermi surface in Mo_8Ga_{41} by quantum oscillations. Our results show three-dimensional characteristics of bands that exhibit strong coupling with phonons and contribute to the larger gap below superconducting T_c. Given relatively high superconducting critical temperature, further studies on the superconducting state and search for similar materials are highly desirable.

This work was supported by the U.S. DOE-BES, Division of Materials Science and Engineering, under Contract No. DE-SC0012704 (BNL). The work at the National High Magnetic Field Laboratory was supported by NSF Cooperative Agreement No. DMR-1644779 and by the State of Florida.

DATA AVAILABILITY

The data that support the findings of this study are available from the corresponding author upon reasonable request.

REFERENCES

[1] J. Nagamatsu, N. Nakagawa, T. Muranaka, Y. Zenitani, and J. Akimitsu, Nature **410**, 63 (2001).
[2] S. L. Bud'ko, G. Lapertot, C. Petrovic, C. E. Cunningham, N. Anderson, and P. C. Canfield, Phys. Rev. Lett. **86**, 1877 (2001).
[3] A. P. Drozdov, M. I. Eremets, I. A. Troyan, V. Ksenofontov, and S. I. Shylin, Nature **525**, 73 (2015).
[4] A. P. Drozdov, P. P. Kong, V. S. Minkov, S. P. Besedin, M. A. Kuzovnikov, S. Mozaffari, L. Balicas, F. F. Balakirev, D. E. Graf, V. B. Prakapenka, E. Greenberg, D. A. Knyazev, M. Tkacz, and M. I. Eremets, Nature **569**, 528 (2019).
[5] I. Errea, M. Calandra, C. J. Pickard, J. Nelson, R. J. Needs, Y. Li, H. Liu, Y. Zhang, Y. Ma, and F. Mauri, Phys. Rev. Lett. **114**, 157004 (2015).
[6] D. J. Scalapino, Rev. Mod. Phys. **84**, 1383 (2012).
[7] A. Bezinge, K. Yvon, M. Decroux, and J. Muller, J. Less-Common Met. **99**, L27 (1984).
[8] J. S. Slusky, N. Rogado, K. A. Regan, M. A. Hayward, P. Khalifah, T. He, K. Inumaru, S. M. Loureiro, M. K. Haas, H. W. Zandbergen, and R. J. Cava, Nature **410**, 343 (2001).
[9] W. Xie, H. Luo, B. F. Phelan, T. Klimczuk, F. A. Cevallos, and R. J. Cava, Proc. Natl. Acad. Sci. U. S. A. **112**, E7048 (2015).
[10] V. Y. Verchenko, A. A. Tsirlin, A. O. Zubtsovskiy, and A. V. Shevelkov, Phys. Rev. B **93**, 064501 (2016).
[11] V. Y. Verchenko, R. Khasanov, Z. Guguchia, A. A. Tsirlin, and A. V. Shevelkov, Phys. Rev. B **96**, 134504 (2017).
[12] A. P. Neha, P. Sivaprakash, K. Ishigaki, G. Kalaiselvan, K. Manikandan, R. S. Dhaka, Y. Uwatoko, S. Arumugam, and S. Patnaik, Mater. Res. Express **6**, 016002 (2018).
[13] A. Sirohi, S. Saha, P. Neha, S. Das, S. Patnaik, T. Das, and G. Sheet, Phys. Rev. B **99**, 054503 (2019).
[14] M. Marcin, J. Kacmarcik, Z. Pribulova, M. Kopcik, P. Szabo, O. Sofranko, T. Samuely, V. Vano, C. Marcenat, V. Y. Verchenko, A. V. Shevelkov, and P. Samuely, Sci. Rep. **9**, 13552 (2019).
[15] D. C. Larbalestier, L. D. Cooley, M. O. Rikel, A. A. Polyanskii, J. Jiang, S. Patnaik, X. Y. Cai, D. M. Feldmann, A. Gurevich, A. A. Squitieri, M. T. Naus,

C. B. Eom, E. E. Hellstrom, R. J. Cava, K. A. Regan, N. Rogado, M. A. Hayward, T. He, J. S. Slusky, P. Khalifah, K. Inumaru, and M. Haas, Nature **410**, 186 (2001).
[16]C. Bergemann, A. P. Mackenzie, S. R. Julian, D. Forsythe, and E. Ohmichi, Adv. Phys. **52**, 639 (2003).
[17]S. E. Sebastian, N. Harrison, and G. G. Lonzarich, Rep. Prog. Phys. **75**, 102501 (2012).
[18]S. E. Sebastian and C. Proust, Annu. Rev. Condens. Matter Phys. **6**, 411 (2015).
[19]C. Proust and L. Taillefer, Annu. Rev. Condens. Matter Phys. **10**, 409 (2019).
[20]C. Buzea and T. Yamashita, Supercond. Sci. Technol. **14**, R115 (2001).
[21]S. Jin, H. Mavoori, C. Bower, and R. B. van Dover, Nature **411**, 563 (2001).
[22]Z. Fisk and J. P. Remeika, "Growth of single crystals from molten metal fluxes," in *Handbook on the Physics and Chemistry of Rare Earths*, edited by K. A. Gschneidner, Jr. and L. Eyring (Elsevier, Amsterdam, 1989), Vol. 12, pp. 53—70.
[23]K. Yvon, Acta Crystallogr., Sect. B **31**, 117 (1975).
[24]E. M. Lifshits and A. M. Kosevich, J. Phys. Chem. Solids **4**, 1 (1958).
[25]D. Shoeneberg, *Magnetic Oscillation in Metals* (Cambridge University Press, Cambridge, 1984).
[26]W. Xia, X. Shi, Y. Wang, W. Ge, H. Su, Q. Wang, X. Wang, N. Yu, Z. Zou, Y. Hao, W. Zhao, and Y. Guo, Appl. Phys. Lett. **116**, 142103 (2020).
[27]W. Xia, X. Shi, Y. Zhang, H. Su, Q. Wang, L. Ding, L. Chen, X. Wang, Z. Zou, N. Yu, L. Pi, Y. Hao, B. Li, Z. Zhu, W. Zhao, X. Kou, and Y. Guo, Phys. Rev. B **101**, 155117 (2020).
[28]B. J. Lawson, G. Li, F. Yu, T. Asaba, C. Tinsman, T. Gao, W. Wang, Y. S. Hor, and L. Li, Phys. Rev. B **90**, 145141 (2014).